Science of the Total Environment 648 (2019) 1394–1402

Contents lists available at ScienceDirect

Science of the Total Environment

journal homepage: www.elsevier.com/locate/scitotenv

Satellite-based regional warming hiatus in China and its implication

Long Li, Yong Zha *

Jiangsu Center for Collaborative Innovation in Geographical Information Resource Development and Application, Key Laboratory of Virtual Geographic Environment of Ministry of Education, College of Geographic Science, Nanjing Normal University, Nanjing 210023, China

HIGHLIGHTS

- The satellite data is used to investigate regional climate warming.
- Characterizing the spatiotemporal trends in near-surface air temperature in China.
- A regional warming hiatus is diagnosed for the period 2001–2015 in China.
- We estimate the land surface temperature-induced warming during the period.
- Greenhouse gases-induced warming is suppressed by natural variability.

GRAPHICAL ABSTRACT

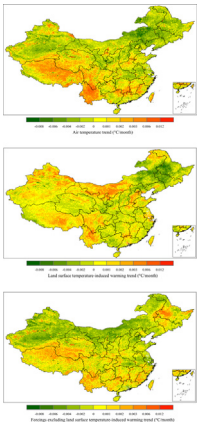

ARTICLE INFO

Article history:
Received 1 May 2018
Received in revised form 17 August 2018
Accepted 17 August 2018
Available online 18 August 2018

Editor: R Ludwig

Keywords:
Climate change
Global warming hiatus
MODIS
Natural variability
Anthropogenic forcing
Remote sensing

ABSTRACT

The slowdown in global warming since 1998, often termed the global warming hiatus. Reconciling the "hiatus" is a main focus in the 2013 climate change conference. Accurately characterizing the spatiotemporal trends in surface air temperature (SAT) is helps to better understand the "hiatus" during the period. This article presents a satellite-based regional warming simulation to diagnose the "hiatus" for 2001–2015 in China. Results show that the rapid warming is mainly in western and southern China, such as Yunnan (mean ± standard deviation: 0.39 ± 0.26 °C (10 yr)$^{-1}$), Tibet (0.22 ± 0.25 °C (10 yr)$^{-1}$), Taiwan (0.21 ± 0.25 °C (10 yr)$^{-1}$), and Sichuan (0.19 ± 0.25 °C (10 yr)$^{-1}$). On the contrary, there is a cooling trend by 0.29 ± 0.26 °C (10 yr)$^{-1}$ in northern China during the recent 15 yr, where a warming rate about 0.38 ± 0.11 °C (10 yr)$^{-1}$ happened for 1960–2000. Overall, satellite simulation shows that the warming rate is reduced to −0.02 °C (10 yr)$^{-1}$. The changes in underlying surface, Earth's orbit, solar radiation and atmospheric counter radiation (USEOSRACR) cause China's temperature rise about 0.02 °C (10 yr)$^{-1}$. A combination of greenhouse gases (GHGs) and other natural forcing (ONAT, predominately volcanic activity, and atmosphere and ocean circulation) explain another part of temperature trend by approximately −0.04 °C (10 yr)$^{-1}$. We conclude that there is a regional warming hiatus, a pause or a slowdown in China, and imply that GHGs-induced warming is suppressed by ONAT in the early 21st century.

© 2018 Elsevier B.V. All rights reserved.

1. Introduction

Global warming "stalled" or "paused" for the period 1998–2012, as claimed by the Intergovernmental Panel on Climate Change (IPCC)

* Corresponding author.
E-mail address: yzha@njnu.edu.cn (Y. Zha).

https://doi.org/10.1016/j.scitotenv.2018.08.233
0048-9697/© 2018 Elsevier B.V. All rights reserved.

Fifth Assessment Report (AR5) (IPCC, 2013). However, the early drafts of IPCC AR5 have no detailed explanation for this "hiatus" since 111 of 114 climate models in the CMIP5 earth system model did not verify this phenomenon. Journalists have more questions on the "global warming hiatus" than other topics at the press conference when the IPCC AR5 was released (Medhaug et al., 2017). Although many researchers made physical explanations for its cause to help to understand the global climate system (Meehl et al., 2013; Kosaka and Xie, 2013; Meehl et al., 2014; England et al., 2014; Tollefson, 2014; Santer et al., 2014; Trenberth and Fasullo, 2014; Schmidt et al., 2014; Watanabe et al., 2013; Fyfe and Gillett, 2014; Ding et al., 2013), only a few scientists (Knight, 2009; Hunt, 2011; Foster and Rahmstorf, 2011; Meehl et al., 2011; Easterling and Wehner, 2009; Robert et al., 2011; Lean and Rind, 2009; Cohen et al., 2012; Meehl and Teng, 2012) confirmed that the observed global warming rate are unusually slow and deviate from the ensemble of climate models (Fyfe et al., 2013). In particular, IPCC stated that residual data deviation during the period could well have weakened recent warming (IPCC, 2013). Some efforts aim to argue the possible artifacts of data biases (Karl et al., 2015), and indicated that these networks of observations included in the previous analysis of IPCC report are always undergoing change; new datasets support the notion that global warming hiatus never happened (Karl et al., 2015). In 2017, after a wave of scientific publications and public debate, the climate models as reported in IPCC remain debates, including definitions of "hiatus" and datasets (Medhaug et al., 2017).

During the periods where natural variability dominates (Meehl et al., 2014) and the role of variations in both natural (Solomon et al., 2011) and anthropogenic forcings (Wilcox et al., 2013), a short term hiatus since the 21st century provides a challenge to more fully and deeply understand the global warming. Compared to the most commonly used climate models for understanding global warming, satellite-based warming simulation provides a new perspective to quantify the spatiotemporal trends in surface air temperature (SAT) and accurately characterize the spatial pattern of warming. The satellite data providing amounts of objectively and spatially contiguous information on the Earth surface can be considered promising in SAT mapping, typically in different spatial scales and various geographic regions (Ho et al., 2014; Zhu et al., 2013; Chen et al., 2015; Benali et al., 2012; Emamifar et al., 2013; Li and Zha, 2018; Zhang et al., 2016; Li et al., 2017; Yoo et al., 2018; Xu et al., 2018). There is a large area of land and broad range of background climate in China that provides a good test platform to investigate regional warming patterns. To our knowledge, few studies accurately characterize the spatiotemporal trends in SAT and further analyze the regional warming pattern during the period of global warming hiatus in China by satellite simulation.

In this research, we establish the underlying relationships between SAT and satellite data, and then quantify the spatiotemporal trend of SAT for 2001–2015 in China. Our aim is to present an analysis combining satellite data with observational data to provide compelling evidence that whether there is a regional hiatus in warming and further analyze the potential causes of a hiatus. We select China, where urbanization is happening at an unprecedented rate (Bai et al., 2014), as a case to conduct an analysis of regional warming hiatus.

2. Methodology

2.1. Weather and satellite data

Weather data can be available from China Meteorological Data Service Center (CMDC), which has strict quality control and measurements using the same standards and instrumentation. These weather stations measured at heights of 2 m above ground, are mainly located in central, eastern and southern China, with an average distance of about 90 km. In this study, we used monthly average SAT during the period from 2001 to 2015. Monthly average SAT was integrated by daily temperature data. CMDC indicates that the data error rate is almost zero by repeated quality inspection and control.

The satellite remote sensing data used in this study involve Moderate Resolution Imaging Spectroradiometer (MODIS) normalized difference vegetation index (NDVI) products (MOD13A3), MODIS land surface temperature (LST) products (MOD11A2), digital elevation model (DEM) and nighttime lights. These widely used products have been proven to be of high quality (Wan, 2008; Peng et al., 2012; Li and Zha, 2018; Zhou et al., 2014). The NDVI products from MODIS Terra (MOD13A3) represented by monthly average NDVI values, and the 8-day composite LST products from MODIS Terra (MOD11A2) monitored at 10:30 h (day) and 22:30 h (night) local solar time were collected for the period 2001–2015 over China. These data were primarily collected from National Aeronautics and Space Administration (NASA). Daytime and nighttime LST products were merged into monthly composites. Cloud-free composite DMSP/OLS nighttime lights data for the period 2001–2013 were freely available from the National Oceanic and Atmospheric Administration's (NOAA) National Geophysical Data Center. DEM was collected from the CGIAR consortium for spatial information with 90 m spatial resolution. Finally, satellite data were resampled into 10 km spatial resolution using bilinear interpolation to render these data consistent with the spatial resolutions used in this study.

2.2. Temperature anomaly modeling

There has been plenty of promising research in SAT mapping across various geographic regions using satellite and other auxiliary data (Chen et al., 2015; Benali et al., 2012; Zhu et al., 2013; Li and Zha, 2018; Ho et al., 2014; Zhang et al., 2016; Li et al., 2017; Yoo et al., 2018; Xu et al., 2018). Among them, LST is the most important predictor in both regional and national temperature estimates (Benali et al., 2012; Yoo et al., 2018; Ho et al., 2014; Emamifar et al., 2013; Chen et al., 2015). Also, to better characterize the spatial distribution of air temperature, many auxiliary data were used to improve model performance. For instance, DEM has been widely used in temperature estimates because of a significant correlation with air temperature (Ho et al., 2014; Chen et al., 2015; Li and Zha, 2018). Air temperature is correlated with NDVI (Piao et al., 2003). Afforestation can decrease the surface temperature by increasing the latent heat flux (Peng et al., 2014; Tran et al., 2006), and has quite different temperature effect in lower and higher latitude regions (Lee et al., 2011). Thus, NDVI as an auxiliary data, in conjunction with the LST was applied to air temperature estimates (Yoo et al., 2018). Night-time light can improve the model performance in air temperature estimates (Li and Zha, 2018), due to its ability to reflect regional effects of human activity on temperature, such as urban heat island effect (Li et al., 2017).

Random forest regression model, using predictors derived from satellite and basic geographic data, was used to establish the underlying relationships between SAT and environmental variables in China (Li and Zha, 2018). Here, we used a random forest regression model to map monthly average SAT during the period 2001–2015 in China, based on daytime LST, nighttime LST, NDVI, DEM and nighttime lights. Sample data (i.e., a combined data of SAT and environmental variables) are divided into two parts including calibration (90% of the sample size) and validation (10% of the sample size). Calibration sets were used to establish the underlying relationships between SAT and environmental variables. Validation sets were used to assess the model performance. A 10-fold cross-validation was conducted to obtain reliable and stable models. We validated the results by quantitative evaluation including accuracy assessment (mean absolute error (MAE) and root-mean-square error (RMSE)) and analysis of frequency distribution.

$$\mathrm{MAE} = \frac{\sum_{i=1}^{n} \left| Y_{obs,i} - Y_{model,i} \right|}{n} \quad (1)$$

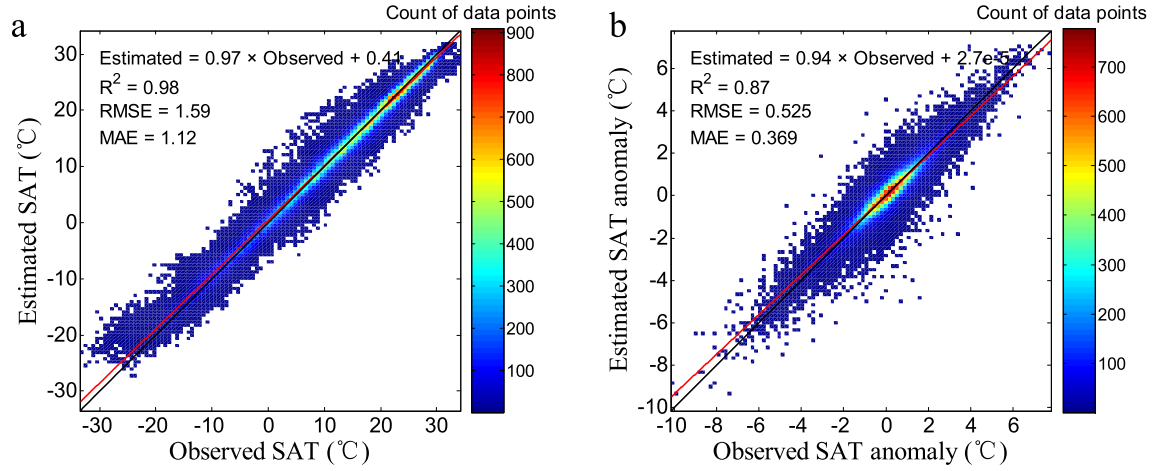

Fig. 1. Density scatterplots show **a** estimated SAT versus observed SAT, **b** estimated SAT anomaly versus observed SAT anomaly. The red line is the linear regression line of best fit. The black line is the 1:1 line of the relationship between x-coordinate and y-coordinate.

$$\mathrm{RMSE} = \sqrt{\frac{\sum_{i=1}^{n}\left(Y_{obs,i} - Y_{model,i}\right)^2}{n}} \quad (2)$$

where $Y_{obs,\,i}$ is the observed SAT (or observed warming rate), $Y_{model,\,i}$ is the predicted SAT (or simulated warming rate), n is the number of meteorological stations. For each pixel, we calculated the time series of monthly average temperature anomaly by subtracting the 15-year monthly average temperature of the corresponding month. Then, we used temperature anomaly time series data to analyze the SAT trend using least squares regression (Ma et al., 2016). We obtained the spatial pattern of regional warming during the periods between 2001 and 2015 in China.

2.3. Driver analysis

Changes in solar radiation, Earth's orbit, volcanic activity, and the atmosphere and ocean circulation are the natural causes of global warming (Meehl et al., 2014; Santer et al., 2015; Nieves et al., 2015). For the full period of our analysis, we calculated the LST anomalies and quantified its trend for 2001–2015. We further calculated the linear correlation between LST anomaly and SAT anomaly. The linear correlation combined with the LST trend was used to analyze the warming caused by the changes in underlying surface, Earth's orbit, solar radiation, and atmospheric counter radiation (related with greenhouse gases, GHGs) (USEOSRACR). Generally, the LST anomalies are directly reflected in the changes of land cover and radiation forcings (Shen et al., 2015). The increase in SAT caused by the increase in LST can reflect the influence of underlying surface, Earth's orbit and solar radiation variabilities on warming and indirect effect of GHGs. Another part of the warming trend could be mainly explained by the influence of GHGs and other natural forcing (ONAT, predominately volcanic activity, and atmosphere and ocean circulation). Therefore, we used a simple method to quantify the combination of GHGs and ONAT induced warming by calculating the difference between total warming rate and USEOSRACR change induced warming rate. Because the heat in the atmosphere mainly comes from the surface, the change in LST is the main driving force of the change in temperature. Compared to the implication of total warming rate, when we exclude the effect of USEOSRACR change on warming, this can better imply the effect of GHGs on warming.

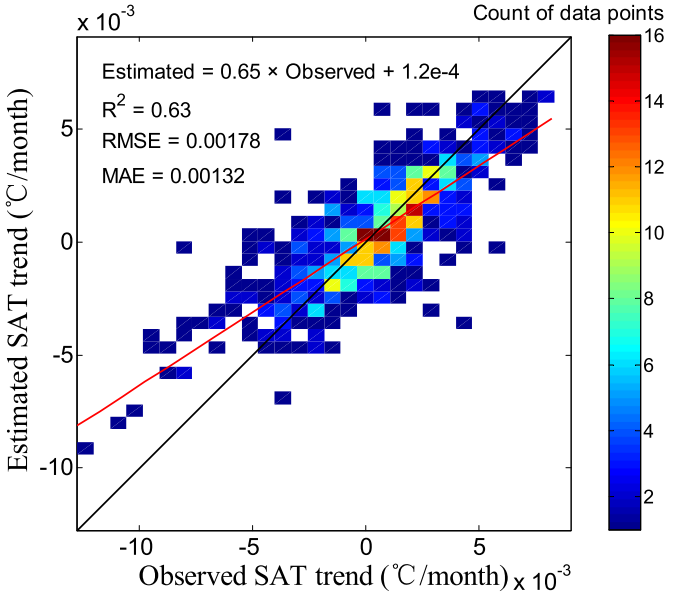
x 10-3
Count of data points
Estimated = 0.65 × Observed + 1.2e-4
R2 = 0.63
RMSE = 0.00178
MAE = 0.00132
Estimated SAT trend (℃/month)
Observed SAT trend (℃/month) x 10-3

Fig. 2. Density scatterplot shows satellite-simulated warming versus observed warming. The red line is the linear regression line of best fit. The black line is the 1:1 line of the relationship between x-coordinate and y-coordinate.

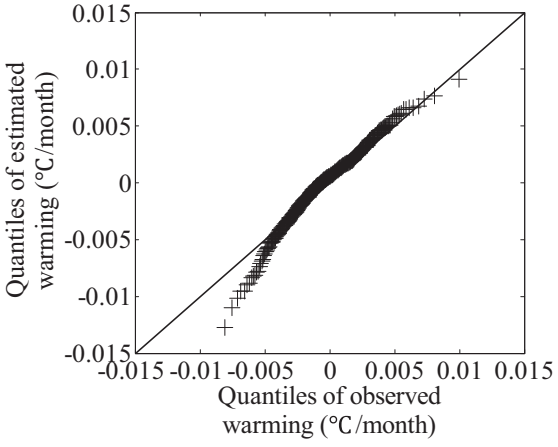

Fig. 3. Q-Q plot shows the relationship between the quantiles of observed warming rate and that of estimated warming rate.

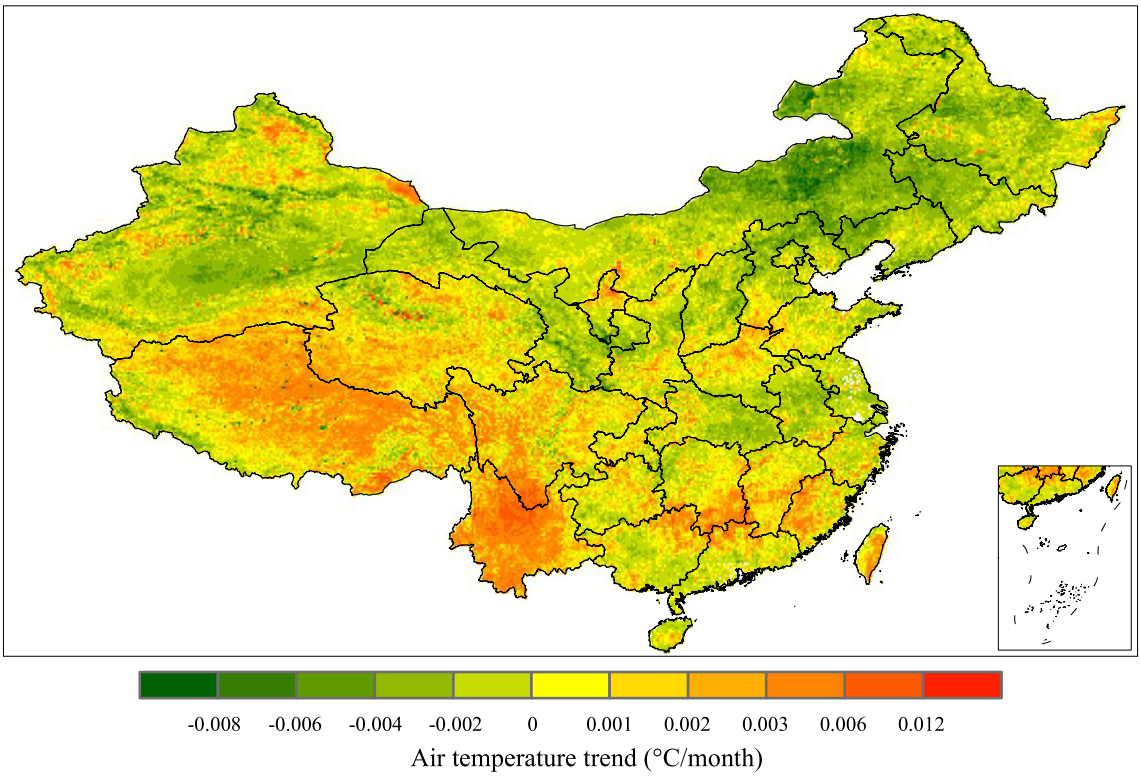

Fig. 4. Satellite-simulated SAT trend for 2001–2015 in China. Red represents temperature rise, and green represents temperature drop. The warming simulation has been validated by analysis of frequency distribution and error estimation.

3. Results and discussion

3.1. Error and uncertainty analysis

Our model produced satisfactory prediction accuracy of SAT simulation (Fig. 1). Fig. 1a shows, the relationship between observed SAT and estimated SAT, that the coefficient of determination (R^2) was as high as 0.98, with a MAE of 1.12 °C and a RMSE of 1.59 °C. Fig. 1b shows, the relationship between observed SAT anomaly and estimated SAT anomaly, that the R^2 was 0.87, with a MAE of 0.369 °C and a RMSE of 0.525 °C. These results indicated that our model could well represent the spatial pattern of SAT and also the change on time (Fig. 1). Next, we simulated the SAT trends and validated the results by quantitative evaluation including accuracy assessment ($R^2 = 0.63$, RMSE = 0.00178 °C/month, MAE = 0.00132 °C/month, Fig. 2) and analysis of frequency distribution. The Q-Q plot shows that simulated warming rate is consistent with the observed warming rate, with almost the same frequency distribution (Fig. 3). The simulated warming matches reasonably well with the trends of observational data (Fig. 4 and Fig. 5). These results provide the reliability of satellite-based SAT trends for further analyzing this regional hiatus.

The error dependencies of simulated warming were evaluated in accordance with the relations between the DEM, land cover, LST coverage rate and model performance (Fig. 6). The model performance was independent of the land cover of weather stations. The majority of weather stations located in low DEM had lower estimated errors compared to the stations located in areas with high DEM. In addition, the coverage of time-series LST products also affected the model performance. When the coverage of time-series LST products was over 70%, the model performance was independent of the coverage. In contrast, there was a significant decrease in model performance if the coverage of time-series LST products was below 70% (Fig. 6).

3.2. Spatial variability estimates in SAT trend

Satellite-simulated warming shows that the trends in average SAT vary spatially for the period 2001–2015 in China (Fig. 4). The rapid warming is mainly in western and southern China, including Yunnan, Tibet, Taiwan, Sichuan, and the adjacent areas of five provinces (i.e., Guangxi, Jiangxi, Fujian, Guangdong, Hunan provinces). The increase in SAT is particularly obvious in Yunnan, with a warming rate about 0.39 ± 0.26 °C $(10\ yr)^{-1}$ (mean ± standard deviation). There is a rapid warming trend about 0.22 ± 0.25 °C $(10\ yr)^{-1}$ on the Tibetan plateau located in Tibet, where warming-induced permafrost thawing and glacier retreat will release substantial carbon dioxide (CO2) and methane (CH4) emissions into the atmosphere (Chen et al., 2013), further exacerbating global warming. Taiwan has a warming rate about 0.21 ± 0.25 °C $(10\ yr)^{-1}$. Also, the average SAT increase by approximately 0.19 ± 0.25 °C $(10\ yr)^{-1}$ in Sichuan. In contrast, it is clear that the average SAT in the north has an inverse trend since the twenty-first century. For example, there is a cooling trend by 0.29 ± 0.26 °C $(10\ yr)^{-1}$ in northern China during the recent 15 years, where a rapid warming about 0.38 ± 0.11 °C $(10\ yr)^{-1}$ (observational data) happened for 1960–2000 (Fig. 5).

In addition to the spatial pattern of warming discussed, we further verify whether there is a regional "hiatus" in China since scientists focus more on the overall trends of SAT during the period (Medhaug et al., 2017; Karl et al., 2015). We used observational data to analyze the spatiotemporal trends in SAT, and find that the warming rate is estimated to be 0.22 °C $(10\ yr)^{-1}$ from 1960 to 2000, but the increasing rate of the SAT is reduced to −0.03 °C $(10\ yr)^{-1}$ for 2001–2015. Further, satellite-based warming shows that the increasing rate of the SAT is reduced to −0.02 °C $(10\ yr)^{-1}$ during this period (Fig. 7), which is very much in accordance with the observed trends in SAT. Not only the observed warming but also the satellite-simulated warming consistently

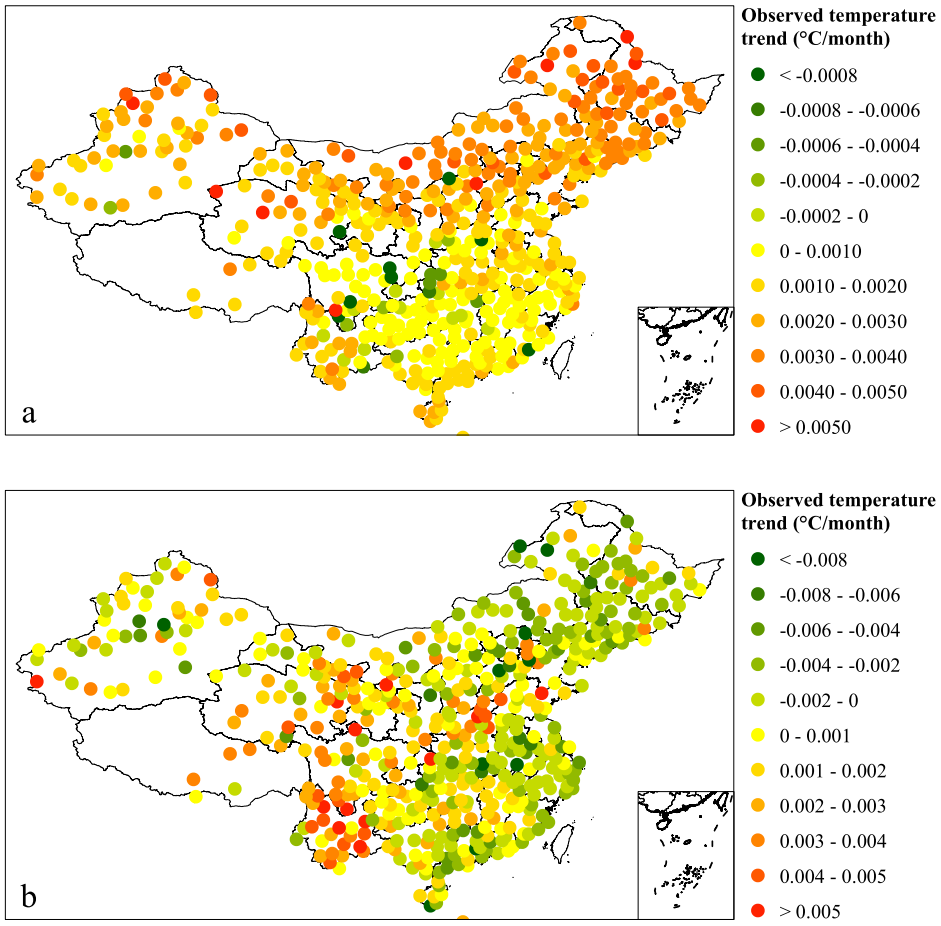

Fig. 5. Location of weather stations and SAT trends for 1960–2015. **a** The SAT trend for the period 1960–2000. **b** The SAT trend for the period 2001–2015.

shows that a regional "hiatus" happened in China in the early 21st century.

3.3. Potential causes of "hiatus"

The linear correlation between SAT anomaly and LST anomaly, and LST trend (Fig. 8) were used to analyze USEOSRACR change induced warming. Result shows that although SAT rises with the increase in LST (average correlative coefficient is 0.66), the contribution of LST to SAT varies spatially. It is more obvious and significant in low-altitude areas and northern China (i.e., same increase in LST causes different SAT rise). SAT rises by more than 0.6 °C with the increase in LST by 1 °C in northern China. SAT rises by less than 0.4 °C with the increase in LST by 1 °C in Qinghai-Tibetan Plateau. SAT in north China rises more than the south China by approximately 0.1 °C with the increase in LST by 1 °C. Overall, the SAT anomaly influenced by the Earth's surface is found more obvious in low-altitude areas and northern China. These results imply the difference in energy transport between SAT anomaly and LST anomaly across different regions.

The effects of the USEOSRACR and a combination of GHGs and ONAT on the SAT trend are depicted in Fig. 9. The cooling trend in northeast China is attributed to a significant decrease of LST, and part of the

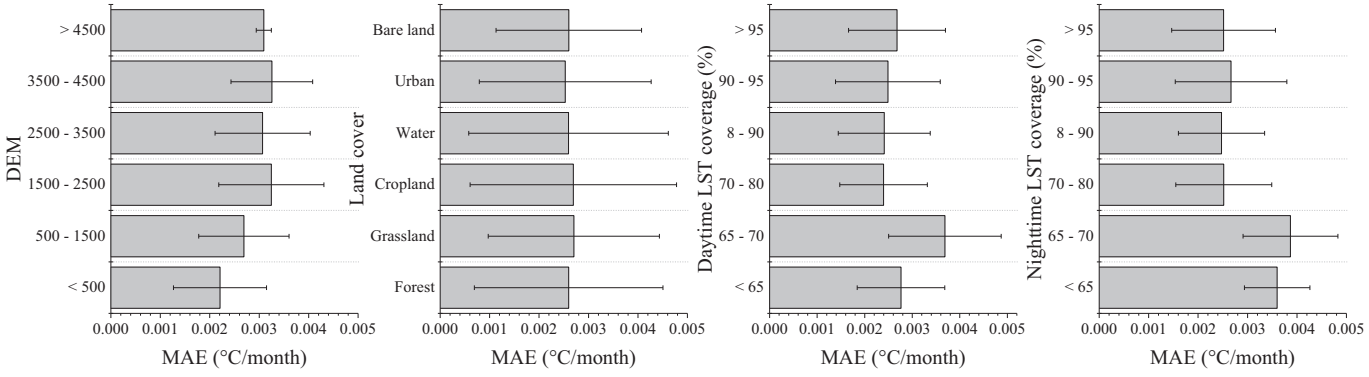

Fig. 6. Relations between the DEM, land cover, LST coverage rate and model performance in simulation of warming.

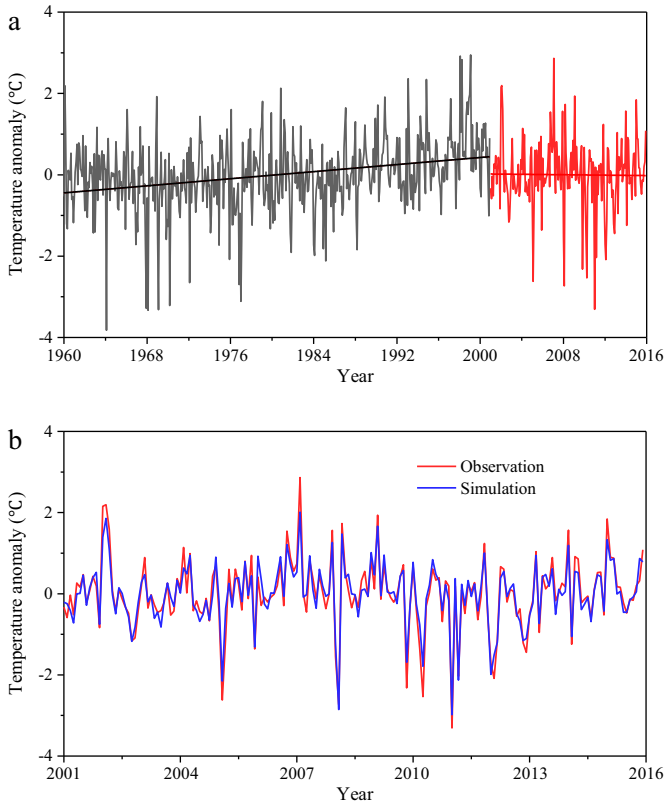

Fig. 7. China's SAT anomaly time series with observed and simulated temperature anomalies. **a** Observed anomaly for 1960–2015 in China. **b** Comparison between observed anomaly and simulated anomaly for the period 2001–2015 in China.

compensation from the combination of GHGs and ONAT. In contrast, the increase of SAT in the Qinghai-Tibetan Plateau is due to a combination of USEOSRACR, GHGs and ONAT changes induced warming. The SAT in northeast China is significantly impacted by the combination of GHGs and ONAT. These findings have implication for the dominant role of natural variability in regional cooling. Studies indicated that the warming rate of Arctic is twice the global average (Serreze and Barry, 2011). The large-amplitude climatic change happened in Qinghai-Tibetan Plateau with a rapid warming rate that greater than those for the polar region and the whole world (Chen et al., 2013; IPCC, 2007). Northeast China is the most important agricultural producing fields, and is also the most susceptible to climate change (Liu et al., 2012). However, the drivers of SAT rise was generally used as a whole to analyze (i.e., average effects of a driver on the increase in global or regional air temperature), and relevant studies rarely investigate the spatial variability of ecosystem response to global warming (Sun et al., 2016). We find that the Qinghai-Tibetan Plateau and Northeast China is more vulnerable to a combination of GHGs and ONAT induced warming (Fig. 9b), which confirm the response of ecosystems to global warming, varies spatially.

IPCC stated that global warming is very likely (likelihood above 90%) due to the increase in GHGs. Thus world leaders in December 2015 reached an agreement that the climate warming is limited to less than 2 °C above preindustrial SAT (Tollefson and Kenneth, 2015). To meet this aspiration, international climate mitigation efforts aim to require large and rapid reductions in GHGs (Friedlingstein and Solomon, 2005; Matthews and Caldeira, 2008). Although global SAT has rapidly risen during the previous century, some studies have indicated a slowdown in surface warming rate (Kosaka and Xie, 2013). In addition to the notion of internal change and heat redistribution between the surface and the ocean interior (Nieves et al., 2015), more debates focus on whether GHGs is dominant in the increase of global SAT, because the global average SAT did not seem to increase as much as was expected from increasing GHGs (Medhaug et al., 2017).

A reduced radiative forcing (Solomon et al., 2011), a smaller warming response to GHGs (Lewis, 2013) and possible artifacts of data biases (Karl et al., 2015) were identified as the potential causes of "hiatus". Here we show that the USEOSRACR change causes temperature rise about 0.02 °C (10 yr)$^{-1}$, and a combination of GHGs and ONAT explains another part of temperature trend by about −0.04 °C (10 yr)$^{-1}$. Indeed, increasing GHGs in China should cause more rapid warming, but the SAT rise "stalled" or "paused" in this century. These results indicate that GHGs-induced warming is suppressed by the natural variability, and the ONAT induced cooling exceeds the GHGs-induced warming. Analysis of ocean observations indicated that a "hiatus" is compensated for internal change or a heat redistribution between the surface and the ocean interior (Nieves et al., 2015). Researches have already identified more rapid warming at deeper levels in Pacific (Kosaka and Xie, 2013), Atlantic (Chen and Tung, 2014), and Indian Oceans (Drijfhout et al., 2015). This has implications for the Earth's net radiative forcing and the approximate equality between ocean heat content increases and unbalanced net radiative at the top of the atmosphere (Church et al., 2013). These studies provide the clearest explanation in heat redistribution, and have implication for the dominant role of natural variability. A regional "hiatus" observed in our study could be impacted by the natural variability from atmosphere and ocean circulation.

3.4. Limitations

The research in this paper has some limitations. On the one hand, the time span from 2001 to 2015 in this study is short, given that the hiatus occurred during the period from 1998 to 2013, and MODIS data can only be available after 2000. Therefore, the statistically inferred trend could be sensitive to the select years. Moreover, our results could only imply GHGs induced warming in space, because it was unable to quantify the separate contribution of GHGs and ONAT to warming by calculating the difference between total warming rate and USEOSRACR change induced warming rate.

4. Conclusion

Few studies have attempted to use satellite data to accurately characterize the spatiotemporal trends in near-surface air temperature. Here, we present a satellite-based regional warming simulation during the period of global warming hiatus. The mothed produces low prediction errors that can be considered promising in remote sensing of climate warming (R^2 = 0.63, RMSE = 0.00178 °C/month, MAE = 0.00132 °C/month). Rapid warming occurs in western and southern China, including Tibet Plateau, Yunnan, Sichuan, and Taiwan. A climate cooling occurs in the northern region for 2001–2015, however, in which a rapid warming happened during the periods from 1960 to 2000. In addition, the analysis of SAT trend in China indicates that there is a hiatus, a pause or a slowdown in regional warming. The USEOSRACR change causes slight rise in SAT but the temperature decreases during the periods, which implies that GHGs-induced warming is suppressed by ONAT during the period.

Acknowledgements

This research was funded by the National Natural Science Foundation of China [Grant no. 41671428], the National Key R&D Program of China [Grant no. 2017YFB0503902], Major Science and Technology Program for Water Pollution Control and Treatment [Grant no. 2017ZX07302003], the Postgraduate Research & Practice Innovation

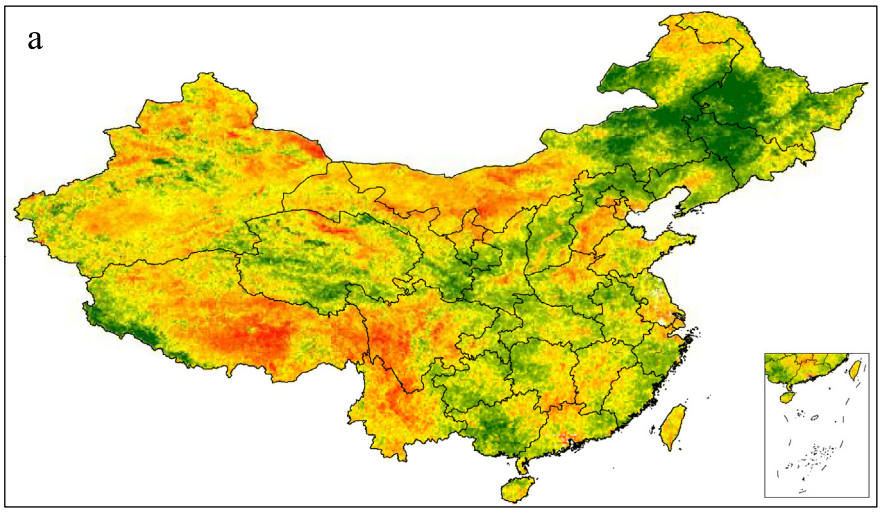
a
-0.007 -0.005 -0.003 -0.001 0 0.001 0.003 0.005 0.007 0.010
Land surface temperature trend (°C/month)

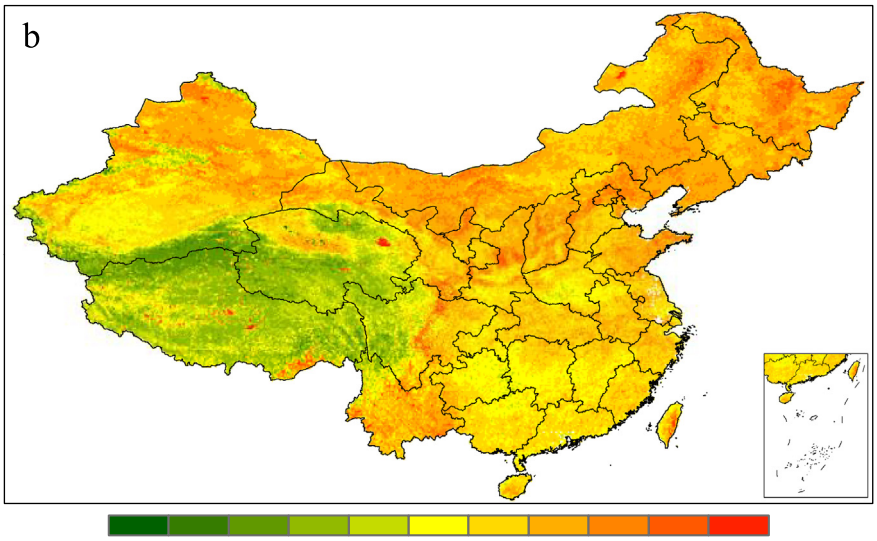
b
0 0.1 0.2 0.3 0.4 0.5 0.6 0.7 0.8 0.9
Slope of the increase in air temperature versus land surface temperature

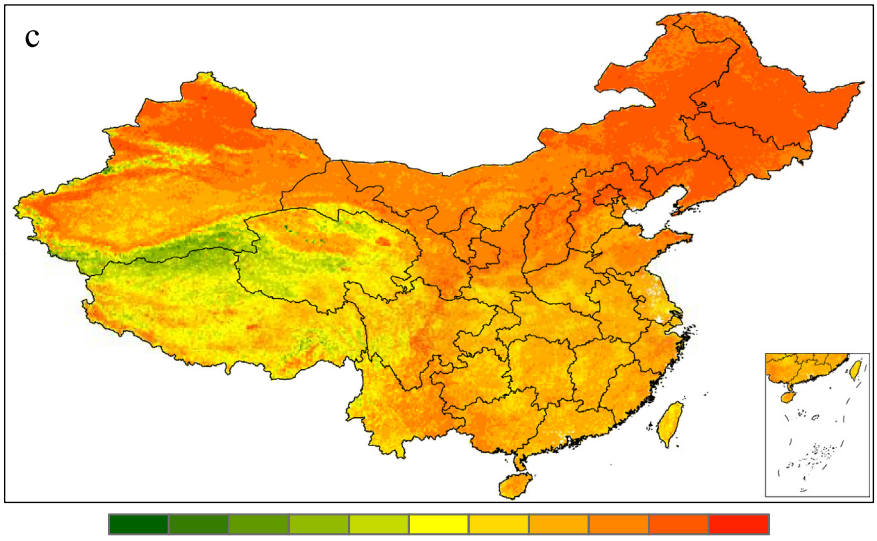
c
0 0.1 0.2 0.3 0.4 0.5 0.6 0.7 0.8 0.9
Correlation coefficient of the increase in air temperature versus land surface temperature

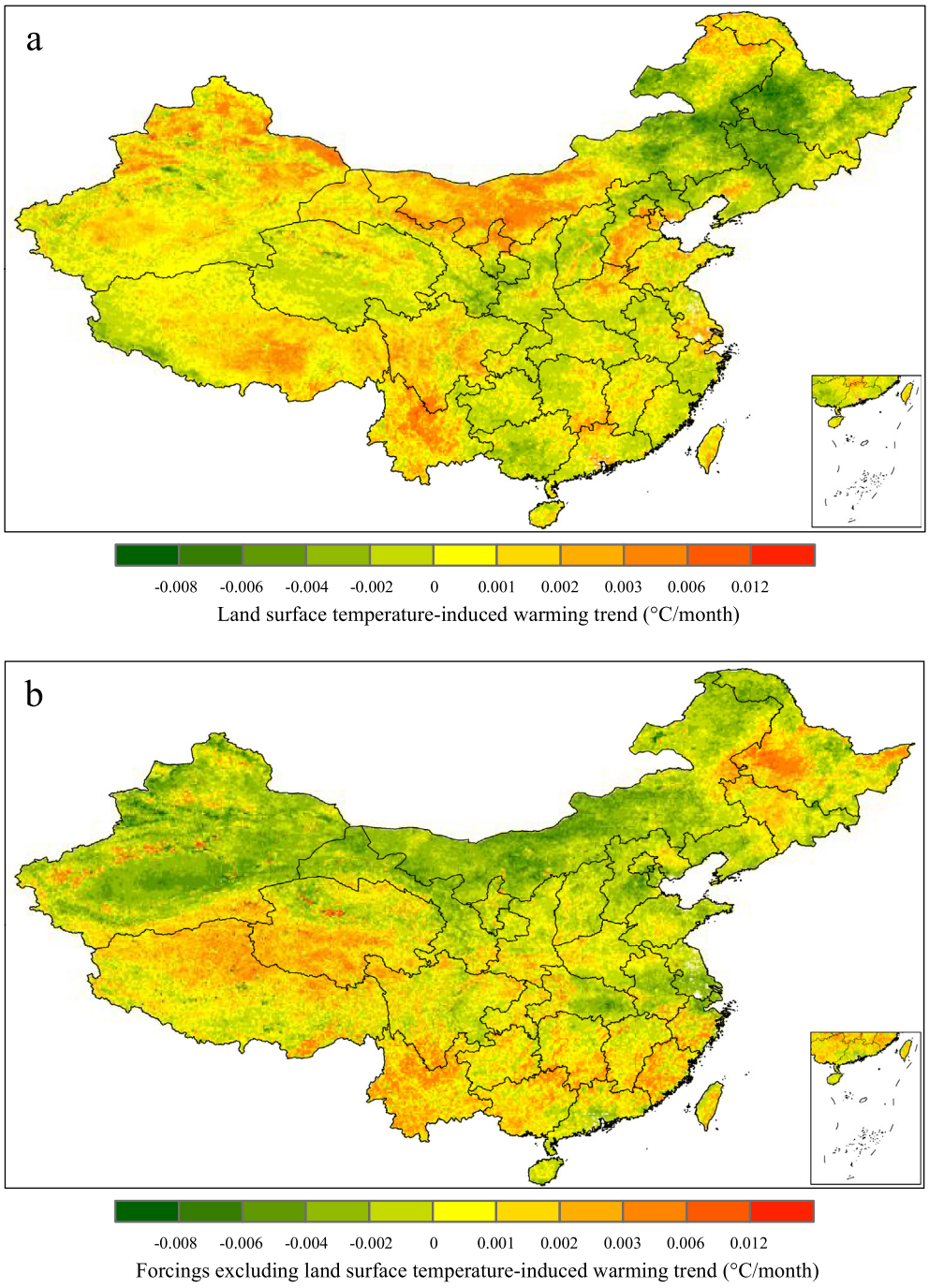
a
-0.008 -0.006 -0.004 -0.002 0 0.001 0.002 0.003 0.006 0.012
Land surface temperature-induced warming trend (°C/month)
b
-0.008 -0.006 -0.004 -0.002 0 0.001 0.002 0.003 0.006 0.012
Forcings excluding land surface temperature-induced warming trend (°C/month)

Fig. 9. Spatial distribution of LST and forcings excluding LST induced warming. **a** LST induced warming trend. **b** forcings excluding LST induced warming trend. LST induced warming reflects the warming caused by the changes in USEOSRACR. Forcings excluding LST are considered as a combination of GHGs and ONAT.

Program of Jiangsu Province [Grant no. KYCX18_1203], and a project funded by the Priority Academic Program Development of Jiangsu Higher Education Institutions, China.

References

Bai, X., Shi, P., Liu, Y., 2014. Realizing China's urban dream. Nature 509, 158–160.
Benali, A., Carvalho, A.C., Nunes, J.P., Carvalhais, N., Santos, A., 2012. Estimating air surface temperature in Portugal using MODIS LST data. Remote Sens. Environ. 124, 108–121.
Chen, X., Tung, K.K., 2014. Climate. Varying planetary heat sink led to global-warming slowdown and acceleration. Science 345, 897.
Chen, H., Zhu, Q., Peng, C., Wu, N., Wang, Y., Fang, X., et al., 2013. The impacts of climate change and human activities on biogeochemical cycles on the Qinghai-Tibetan plateau. Glob. Chang. Biol. 19, 2940–2955.
Chen, F., Liu, Y., Liu, Q., Qin, F., 2015. A statistical method based on remote sensing for the estimation of air temperature in China. Int. J. Climatol. 35, 2131–2143.
Church, J.A., et al., 2013. Revisiting the Earth's sea-level and energy budgets from 1961 to 2008. Geophys. Res. Lett. 40, 4066.
Cohen, J.L., Furtado, J.C., Barlow, M., Alexeev, V.A., Cherry, J.E., 2012. Asymmetric seasonal temperature trends. Geophys. Res. Lett. 39, 54–62.

Fig. 8. LST trend and asymmetric effects of LST change induced warming. **a** LST trend for 2001–2015. **b** The slope of the increase in air temperature versus LST shows the temperature rise with unit LST increase. **c** Correlation coefficient of the increase in air temperature versus LST. Subplots a and b were used to analyze the warming caused by the changes in USEOSRACR.

Ding, H., Greatbatch, R.J., Latif, M., Park, W., Gerdes, R., 2013. Hindcast of the 1976/77 and 1998/99 climate shifts in the pacific. J. Clim. 26, 7650–7661.
Drijfhout, S.S., Blaker, A.T., Josey, S.A., Nurser, A.J.G., Sinha, B., Balmaseda, M.A., 2015. Surface warming hiatus caused by increased heat uptake across multiple ocean basins. Geophys. Res. Lett. 41, 7868–7874.
Easterling, D.R., Wehner, M.F., 2009. Is the climate warming or cooling? Geophys. Res. Lett. 36, 262–275.
Emamifar, S., Rahimikhoob, A., Noroozi, A.A., 2013. Daily mean air temperature estimation from MODIS land surface temperature products based on M5 model tree. Int. J. Climatol. 33, 3174–3181.
England, M.H., Mcgregor, S., Spence, P., Meehl, G.A., Timmermann, A., Cai, W., et al., 2014. Recent intensification of wind-driven circulation in the pacific and the ongoing warming hiatus. Nat. Clim. Chang. 4, 222–227.
Foster, G., Rahmstorf, S., 2011. Global temperature evolution 1979–2010. Environ. Res. Lett. 6, 526–533.
Friedlingstein, P., Solomon, S., 2005. Contributions of past and present human generations to committed warming caused by carbon dioxide. PNAS 102, 10832–10836.
Fyfe, J.C., Gillett, N.P., 2014. Recent observed and simulated warming. Nat. Clim. Chang. 4, 150–151.
Fyfe, J.C., Gillett, N.P., Zwiers, F.W., 2013. Overestimated global warming over the past 20 years. Nat. Clim. Chang. 3, 767–769.
Ho, H.C., Knudby, A., Sirovyak, P., Xu, Y., Hodul, M., Henderson, S.B., 2014. Mapping maximum urban air temperature on hot summer days. Remote Sens. Environ. 154, 38–45.
Hunt, B.G., 2011. The role of natural climatic variation in perturbing the observed global mean temperature trend. Clim. Dyn. 36, 509–521.
IPCC, 2007. Climate change 2007: the physical science basis. In: Contribution of Working Group I to the Fourth Assessment Report of the Intergovernmental Panel on Climate Change, pp. 237–336.
IPCC, 2013. Climate change 2013: the physical science basis. In: Contribution of Working Group I to the Fifth Assessment Report of the Intergovernmental Panel on Climate Change. 5163, pp. 710–719.
Karl, T.R., Arguez, A., Huang, B., Lawrimore, J.H., Mcmahon, J.R., Menne, M.J., et al., 2015. Possible artifacts of data biases in the recent global surface warming hiatus. Science 348, 1469.
Knight, J., 2009. Do global temperature trends over the last decade falsify climate predictions? Bull. Am. Meteorol. Soc. 90.
Kosaka, Y., Xie, S.P., 2013. Recent global-warming hiatus tied to equatorial pacific surface cooling. Nature 501, 403.
Lean, J.L., Rind, D.H., 2009. How will Earth's surface temperature change in future decades? Geophys. Res. Lett. 36, 15708.
Lee, X., Goulden, M.L., Hollinger, D.Y., Barr, A., Black, T.A., Bohrer, G., et al., 2011. Observed increase in local cooling effect of deforestation at higher latitudes. Nature 479, 384–387.
Lewis, N., 2013. An objective bayesian improved approach for applying optimal fingerprint techniques to estimate climate sensitivity. J. Clim. 26, 7414–7429.
Li, L., Zha, Y., 2018. Mapping relative humidity, average and extreme temperature in hot summer over China. Sci. Total Environ. 615, 875.
Li, L., Huang, X., Li, J., Wen, D., 2017. Quantifying the spatiotemporal trends of canopy layer heat island (CLHI) and its driving factors over Wuhan, China with satellite remote sensing. Remote Sens. 9, 536.
Liu, Z., Yang, X., Hubbard, K.G., Lin, X., 2012. Maize potential yields and yield gaps in the changing climate of Northeast China. Glob. Chang. Biol. 18, 3441–3454.
Ma, Z., Hu, X., Sayer, A.M., Levy, R., Zhang, Q., Xue, Y., et al., 2016. Satellite-based spatiotemporal trends in PM2.5 concentrations: China, 2004–2013. Environ. Health Perspect. 124, 184–192.
Matthews, H.D., Caldeira, K., 2008. Stabilizing climate requires near-zero emissions. Geophys. Res. Lett. 35, 339–356.
Medhaug, I., Stolpe, M.B., Fischer, E.M., Knutti, R., 2017. Reconciling controversies about the 'global warming hiatus. Nature 545, 41.
Meehl, G.A., Teng, H., 2012. Case studies for initialized decadal hindcasts and predictions for the pacific region. Geophys. Res. Lett. 39, 22705.
Meehl, G.A., Arblaster, J.M., Fasullo, J.T., Hu, A., Trenberth, K.E., 2011. Model-based evidence of deep-ocean heat uptake during surface-temperature hiatus periods. Nat. Clim. Chang. 1, 360–364.
Meehl, G.A., Hu, A., Arblaster, J.M., Fasullo, J., Trenberth, K.E., 2013. Externally forced and internally generated decadal climate variability associated with the interdecadal pacific oscillation. J. Clim. 26, 7298–7310.
Meehl, G.A., Teng, H., Arblaster, J.M., 2014. Climate model simulations of the observed early-2000s hiatus of global warming. Nat. Clim. Chang. 4, 898–902.
Nieves, V., Willis, J.K., Patzert, W.C., 2015. Global warming. Recent hiatus caused by decadal shift in indo-pacific heating. Science 349, 532.
Peng, S., Piao, S., Ciais, P., Friedlingstein, P., Ottle, C., Bréon, F.M., et al., 2012. Surface urban heat island across 419 global big cities. Environ. Sci. Technol. 46, 696–703.
Peng, S.S., Piao, S., Zeng, Z., Ciais, P., Zhou, L., Li, L.Z., et al., 2014. Afforestation in China cools local land surface temperature. Proc. Natl. Acad. Sci. U. S. A. 111, 2915–2919.
Piao, S., Fang, J., Zhou, L., Guo, Q., Henderson, M., Ji, W., et al., 2003. Interannual variations of monthly and seasonal normalized difference vegetation index (NDVI) in China from 1982 to 1999. J. Geophys. Res.-Atmos. 108, 1 ACL.
Robert, K.K., Heikki, K., Michael, L.M., James, H.S., 2011. Reconciling anthropogenic climate change with observed temperature 1998–2008. PNAS 108, 11790–11793.
Santer, B.D., Bonfils, C., Painter, J.F., Zelinka, M.D., Mears, C., et al., 2014. Volcanic contribution to decadal changes in tropospheric temperature. Nat. Geosci. 7, 185–189.
Santer, B.D., Solomon, S., Bonfils, C., Zelinka, M.D., Painter, J.F., Beltran, F., et al., 2015. Observed multivariable signals of late 20th and early 21st century volcanic activity. Geophys. Res. Lett. 42, 500–509.
Schmidt, G.A., Shindell, D.T., Tsigaridis, K., 2014. Reconciling warming trends. Nat. Geosci. 7, 158–160.
Serreze, M.C., Barry, R.G., 2011. Processes and impacts of arctic amplification: a research synthesis. Glob. Planet. Chang. 77, 85–96.
Shen, G., Ibrahim, A.N., Wang, Z., Ma, C., Gong, J., 2015. Spatial–temporal land-use/land-cover dynamics and their impacts on surface temperature in Chongming Island of Shanghai, China. Int. J. Remote Sens. 36, 4037–4053.
Solomon, S., Daniel, J.S., Vernier, J.P., Dutton, E.G., Thomason, L.W., 2011. The persistently variable "background" stratospheric aerosol layer and global climate change. Science 333, 866–870.
Sun, Y., Zhang, X., Ren, G., Zwiers, F.W., Hu, T., 2016. Contribution of urbanization to warming in China. Nat. Clim. Chang. 6, 706–709.
Tollefson, J., 2014. Climate change: the case of the missing heat. Nature 505, 276.
Tollefson, J.W., Kenneth, R., 2015. Nations approve historic global climate accord. Nature 528, 315.
Tran, H., Uchihama, D., Ochi, S., Yasuoka, Y., 2006. Assessment with satellite data of the urban heat island effects in Asian mega cities. Int. J. Appl. Earth Obs. Geoinf. 8, 34–48.
Trenberth, K.E., Fasullo, J., 2014. Earth's energy imbalance. J. Clim. 27, 3129–3144.
Wan, Z., 2008. New refinements and validation of the MODIS land-surface temperature/emissivity products. Remote Sens. Environ. 112, 59–74.
Watanabe, M., Kamae, Y., Yoshimori, M., Oka, A., Sato, M., Ishii, M., et al., 2013. Strengthening of ocean heat uptake efficiency associated with the recent climate hiatus. Geophys. Res. Lett. 40, 3175–3179.
Wilcox, L.J., Highwood, E.J., Dunstone, N.J., 2013. The influence of anthropogenic aerosol on multi-decadal variations of historical global climate. Environ. Res. Lett. 8, 279–288.
Xu, Y., Knudby, A., Shen, Y., Liu, Y., 2018. Mapping monthly air temperature in the Tibetan plateau from MODIS data based on machine learning methods. IEEE J-STARS 99, 1–10.
Yoo, C., Im, J., Park, S., Quackenbush, L.J., 2018. Estimation of daily maximum and minimum air temperatures in urban landscapes using MODIS time series satellite data. ISPRS J. Photogramm. Remote Sens. 137, 149–162.
Zhang, H., Zhang, F., Ye, M., Che, T., Zhang, G., 2016. Estimating daily air temperatures over the Tibetan plateau by dynamically integrating MODIS LST data. J. Geophys. Res.-Atmos. 121 (19), 11425–11441.
Zhou, D., Zhao, S., Liu, S., Zhang, L., Chao, Z., 2014. Surface urban heat island in china's 32 major cities: spatial patterns and drivers. Remote Sens. Environ. 152, 51–61.
Zhu, W., Lű, A., Jia, S., 2013. Estimation of daily maximum and minimum air temperature using MODIS land surface temperature products. Remote Sens. Environ. 130, 62–73.